




# Sensitive and selective detection of DNA fragments associated with *Ganoderma boninense* by DNA-nanoparticle conjugate hybridisation

Ekta Rani<sup>1</sup>, Siti Akhtar Mohshim<sup>2,3</sup>, Nor Hidayat Yusof<sup>4</sup>, Muhammad Zamharir Ahmad<sup>2</sup>, Royston Goodacre<sup>1,5</sup>, Shahrul Ainliah Alang Ahmad<sup>3,4</sup>, and Lu Shin Wong<sup>1,\*</sup> 

<sup>1</sup> Manchester Institute of Biotechnology and School of Chemistry, University of Manchester, 131 Princess Street, Manchester M1 7DN, UK

<sup>2</sup> Biotechnology and Nanotechnology Research Centre, Malaysian Agricultural Research and Development Institute, 43400 Serdang, Selangor, Malaysia

<sup>3</sup> Institute of Advanced Technology, Universiti Putra Malaysia (UPM), 43400 Serdang, Selangor, Malaysia

<sup>4</sup> Department of Chemistry, Faculty of Science, Universiti Putra Malaysia, 43400 Serdang, Selangor, Malaysia

<sup>5</sup> Department of Biochemistry, Institute of Integrative Biology, University of Liverpool, Crown Street, Liverpool L69 7ZB, UK

Received: 4 May 2020

Accepted: 5 July 2020

Published online:

20 July 2020

© The Author(s) 2020

## ABSTRACT

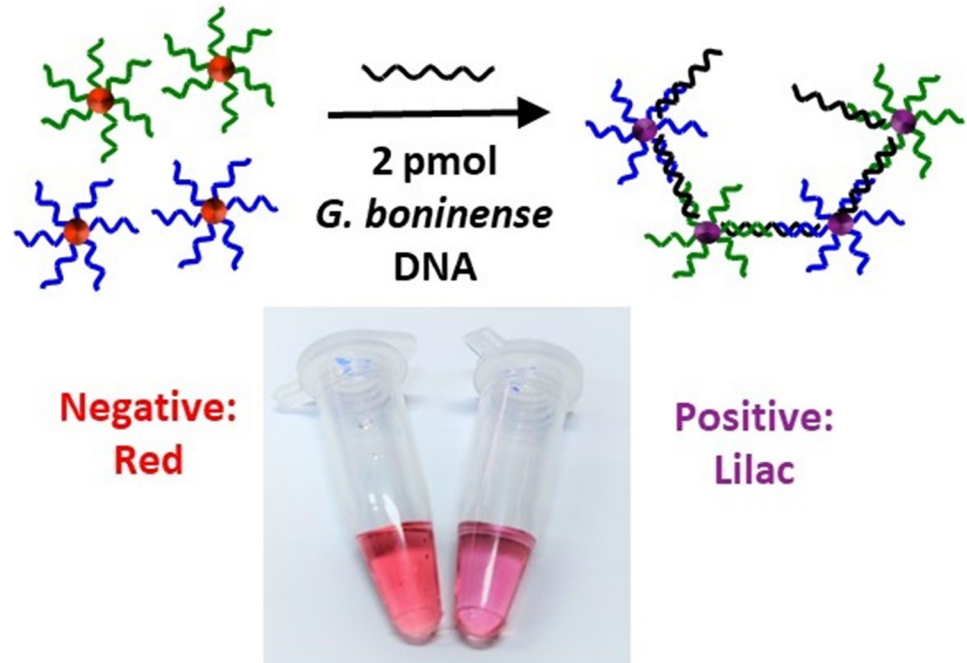
A colourimetric assay for the detection of DNA fragments associated with the oil palm pathogen *Ganoderma boninense* and other fungi DNA is reported. The assay is based on the aggregation of DNA-nanoparticle conjugates in the presence of complementary DNA from the target organism. Here, various designs of DNA-nanoparticle conjugates were evaluated, and it was found that the best design gave a visually observable colour change with as little as 2 pmol of double-stranded DNA analyte even in the presence of a large excess of a mixture of non-complementary DNA. Overall, this label-free system is rapid, sensitive, selective, simple in design, and easy to carry out. It does not require specialist equipment or specialist training for the interpretation of the results, and therefore has the potential to be deployed for agricultural diagnostics in the field.

Address correspondence to E-mail: l.s.wong@manchester.ac.uk

<https://doi.org/10.1007/s10853-020-05058-8>

## GRAPHIC ABSTRACT

Development of a colourimetric assay based on DNA-nanoparticle conjugates for the oil palm pathogen *Ganoderma boninense*.



## Introduction

The oil palm *Elaeis guineensis* is the most important cash crop in Malaysia, which generated an annual export income of RM 65 billion (~ US\$ 16 billion) in 2016 [1]. However, the yearly harvest is substantially reduced by basal stem rot (BSR) disease, caused by infections of pathogenic fungi of the *Ganoderma* sp., and in particular *Ganoderma boninense* [2–6]. BSR causes a reduction in crop yields and eventual death of the palms, necessitating frequent felling and replanting. As a result, BSR causes economic losses of between RM 225 million and RM 1.5 billion annually in Malaysia alone [7]. Since there is no effective treatment for BSR once it manifests, management of the disease revolves around the isolation of infected plants (e.g. by trenching, ploughing, or harrowing the soil around the palm) [2]. As with any transmissible disease, early detection of infection is key to this management strategy. However, such detection is currently difficult since *Ganoderma* is a soil-borne

organism that is transmitted through the roots of young plants, and the disease is symptomless at the early stage of infection. Thus, there is a need for quantitative, sensitive, and selective detection methods. Furthermore, for any diagnostic system to be applicable for use in the field, it must also ideally be portable, affordable, have low power consumption, be tolerant to a wide range of environmental conditions, and not dependent on specialist equipment or training.

Various physical and chemical methods based on volatile molecule “electronic-nose” sensors [8], ultrasonic density measurements [9], spectral imaging [10–12], and microwave radar backscattering [13] have been investigated in attempts to detect *G. boninense* in the field. However, these detection methods possess practical disadvantages regarding complexity, cost and the need for specialist equipment and training to interpret the data. From a molecular biological perspective, the earliest molecular attempts to identify *G. boninense* species relied on antibody-based

immunoassays [14–16]. However, due to the cross-reactivity of the antibodies, false-positive results caused by other fungi such as *Trichoderma* and *Botrytis* species, were also observed [15]. Further, their application in routine analysis is limited by their complex protocols, labile reagents with high cost, relatively low sensitivity, and the requirement of highly skilled personnel. Electrochemical methods for the detection of quinoline (a secondary metabolite produced by the palms under *Ganoderma* attack) [17] and DNA fragments associated with this organism [18, 19] have also been reported. The latter, in particular, has been shown to give high sensitivity (5 mL of analyte at  $\sim 1$  fM of target DNA) and selectivity towards *G. boninense*. However, these methods rely on electrodes that are somewhat complex to fabricate and still rely on trained personnel for data analysis and interpretation.

In contrast, colourimetric assays that employ gold nanoparticles (AuNP) conjugated to DNA [20–28] have shown great potential in diagnostics for human diseases [29, 30]. Here, the presence of an analyte DNA strand bearing a sequence complementary to the DNA on the AuNP results in hybridisation of the DNA and concomitant aggregation of the nanoparticles. This aggregation gives rise to an increase in the particles' surface plasmon resonance and thus UV–Vis absorption spectrum (i.e. an increase in  $\lambda_{\max}$  of the spectrum), which translates into a visually observable colour change (typically red to lilac). Indeed, visible colour changes upon nanoparticle aggregation have been used in other areas, including trace metal analysis in water testing [31]. This analytical approach, therefore, offers many of the attributes that are desirable in a diagnostic system and would be applicable to field use, being portable, easy to carry out (only simple manipulations and without specialist equipment), and interpret.

Herein, we report a methodology for the application of DNA–AuNP conjugates towards the detection and quantification of DNA sequences related to *G. boninense* and other fungal DNA, in the context of single- and double-stranded DNA analytes, as well as in the presence of a mixture of non-complementary DNA. Furthermore, these procedures have been carried out independently in the UK (Manchester) and Malaysia (UPM) to demonstrate their reproducibility.

## Materials and methods

### Materials and equipment

All chemical reagents were purchased from Sigma-Aldrich (now Merck) or ThermoFisher Scientific and used as supplied. All reagents were of analytical grade. 20-nm AuNP colloid at a concentration of 1 optical density (OD) unit @ 525 nm in  $0.1 \text{ mg mL}^{-1}$  sodium citrate was purchased from Alfa Aesar (Heysham, UK). Deionised water (resistivity  $\sim 18.2 \text{ M}\Omega$ ) was used in all cases.

The single-stranded (ss) DNA, double-stranded (ds) DNA of the analyte sequences and various DNA probes (with a 5' S–S C6 disulfide linker or 3' S–S C3 disulfide linker) were purchased from Sigma-Aldrich. These were supplied after purification by high-performance liquid chromatography and in lyophilised form. Deoxyribonucleic acid sodium salt from calf thymus (referred henceforth as “CT”) was supplied by Sigma-Aldrich.

### Preparation of DNA–AuNP conjugates

The DNA–AuNP conjugates were prepared using a general procedure previously described [32] with few modifications. Aqueous solutions of disulfide-functionalised oligonucleotides ( $100 \mu\text{M}$ ,  $40 \mu\text{L}$ ) and tris(2-carboxyethyl)phosphine ( $20 \text{ mM}$ ,  $40 \mu\text{L}$ ) were combined and incubated for 2 h at room temperature (RT) to prepare  $50 \mu\text{M}$  solutions of the oligonucleotides with reduced thiols. This solution ( $80 \mu\text{L}$ ) was then mixed with 1 mL of citrate stabilised AuNP colloid, and the mixture was incubated at RT for 12 h.  $24 \mu\text{L}$  of 1 M NaCl was added to this mixture, followed by sonication for 10 s. The NaCl addition and sonication were repeated four times at 1 h intervals (i.e. 5 times in total) until a final concentration of 0.1 M NaCl was achieved. The final colloidal solution was allowed to stand at RT for 24 h and then centrifuged at  $19000 \text{ g}$  for 30 min. The supernatant was decanted, and the pellet of AuNP resuspended in phosphate-buffered saline (PBS) diluted to half-strength (i.e. final composition  $5.9 \text{ mM}$  phosphate buffer,  $68.5 \text{ nM}$  NaCl,  $1.35 \text{ mM}$  KCl, pH 7.4) containing 0.01% v/v Tween 20. This process of centrifugation, decanting, and resuspension was carried out three times in total, with the final pellet of AuNP being re-suspended in  $100 \mu\text{L}$  of 10 mM PBS buffer. The OD was then measured by UV–Vis spectroscopy

at 525 nm. These DNA-AuNP conjugates were typically stored at 4 °C and used within a week of preparation. Prior to use, the OD of each colloid was adjusted to 0.7 by the addition of the relevant volume of PBS.

### Hybridisation assay

Lyophilised analyte ssDNA and dsDNA were reconstituted in water to make up two stock solutions of either 5 or 1 µM. The more concentrated stock solution was used in experiments requiring a higher analyte final concentration of 200 pmol, while the more dilute solution was used for all other experiments.

#### Assays with ssDNA

40 µL of each DNA-AuNP conjugate was mixed with 10 µL of hybridisation buffer (10 mM phosphate buffer, pH 7.0 with 0.3 M NaCl). The analyte ssDNA stock solutions were then added in volumes appropriate to make up the desired analyte final concentration. To these mixtures, 40 µL of NaCl solution of 5 M was added (to achieve a final concentration of 1 M in the assay mixture). Finally, water was added to make up the final assay volume to 200 µL. This assay mixture was heated to 95 °C for 2 min, followed by gradual cooling (approximate rate of cooling was 5 °C min<sup>-1</sup>) to RT (25–30 °C) over approximately 15 min.

#### Assays with dsDNA

To prepare the working analyte solutions, the dsDNA stock solutions (at volumes to make up the desired analyte concentration in 200 µL) were diluted with water to a total volume of 70 µL. These mixtures were heated at 95 °C for 2 min, and to this heated solution, a mixture of DNA-AuNP conjugates (40 µL each) and 10 µL of hybridisation buffer (see above for composition) was added. To these mixtures, 40 µL of NaCl solution of either 5.0 or 6.1 M was added to achieve a final NaCl concentration in the assay mixture of 1, or 1.2 M, respectively, and a final volume of 200 µL. This assay was again heated at 95 °C for 2 min, followed by gradual cooling to RT over approximately 30 min.

#### Detection of dsDNA in a mixture of calf-thymus DNA

To prepare the working analyte solutions, the dsDNA stock solutions (at volumes to make up the desired analyte concentration in 200 µL) were mixed with water to a volume of 68 µL. 2 µL of calf-thymus DNA solution (100 mg/77 µL in water) was added. The rest of the procedure was followed as noted in “Assays with dsDNA” section

## Results and discussion

### Preparation and stability of DNA-AuNP conjugates

As targets for detection, 35-base DNA sequences from the internal transcribed spacer 1 (ITS1) region of fungal 18S ribosomal genes were chosen. For the species-selective detection of *G. boninense*, the target sequence was taken from a gene bearing the NCBI GenBank accession number EU701010 [5] (termed T1, Table 1). A second sequence taken from the accession number BD082757 [5, 33] (termed T2) was also chosen, which was a match not only to *G. boninense* but also a wider range of fungal ITS1 genes and served as a more general target for the detection fungi of the Basidiomycota phylum [34].

Pairs of DNA-AuNP conjugates bearing complementary probe DNA sequences to each target were prepared. Two general assay configurations were investigated for each target. In the “head-to-tail” (HTT) [20] configuration, two probes in series were employed, with each complementary probe sequence attached at 5'-end to the AuNP via a 12 base GC repeat spacer and an alkylthiol linker (Fig. 1a). Here, a GC spacer [35] is used to increase the distance between the AuNPs and the target complementary DNA sequences, to address potential steric crowding during hybridisation. In the “tail-to-tail” (TTT) format [22], one probe sequence was attached at the 5'-end and the other via the 3'-end, and the DNA sequences were attached directly to the AuNPs via alkylthiol linkers only (Fig. 1b).

To improve the likelihood of identifying probes that would give reliable results, several pairs of DNA-AuNP conjugate probes were prepared for both target sequences. Thus, for target sequence T1, one probe pair in the head-to-tail configuration (termed P1a<sup>HTT</sup> and P1b<sup>HTT</sup>) and two pairs in tail-to-tail

**Table 1** List of DNA sequences used in this study. All the sequences are listed in the 5' to 3' direction. The colour coding is used for clarity and is consistent with that in Fig. 1. The mismatches are underlined for emphasis

Ref.	Description	Sequence (annotated for clarity)	
<b>T1</b>	35-mer sequence corresponding to fragment from NCBI	TTGGCTCTCGCATCGATGAAGAAGAACGCAGCAGG	
	GenBank accession number EU701010		
<b>M1</b>	T1 with single a mismatch	TTGGCTCTCGCATCGAT <u>C</u> AAGAAGAACGCAGCAGG	
<b>P1a<sup>HTT</sup></b> <b>P1b<sup>HTT</sup></b>	DNA probes complementary to T1 in a head-to-tail configuration	<b>Alkylthiol linker Poly-GC Binding sequence</b> (Thiol-C6)GGCCGCGGGCGGCTGCTGCGTTCTTCTTCAT (Thiol-C6)GGCCGCGGGCGGCGATGCGAGAGCCAA	
	<b>P1a<sup>TTT</sup></b> <b>P1b<sup>TTT</sup></b> <b>P1c<sup>TTT</sup></b> <b>P1d<sup>TTT</sup></b>	DNA probes complementary to T1 in a tail-to-tail configuration	(Thiol-C6)CCTGCTGCGTTCTTCTTCAT CGATGCGAGAGCCAA(Thiol-C3) (Thiol-C6)CCTGCTGCGTTCTTC TTCATCGATGCGAGAGCCAA(Thiol-C3)
35-mer sequence corresponding to fragment from NCBI GenBank accession number BD082757		TTGGCTCTCGCATCGATGAAGAACGCAGCGAAATG	
<b>M2</b> <b>M2a</b> <b>M2b</b> <b>M2c</b> <b>M2d</b> <b>M2e</b> <b>M2f</b>		T2 with various mismatch(es)	TTGGCTCTCGCATCGATG <u>G</u> GAGAACGCAGCGAAATG TTGGCTCTCGCATCGATG <u>GGA</u> AACGCAGCGAAATG TTGGCTCTCGCATCGAT <u>AGGAG</u> ACGCAGCGAAATG TTGGCTCTC <u>A</u> CATCGATG <u>G</u> GAGAACGC <u>G</u> GCGAAATG TTG <u>A</u> CTCTC <u>A</u> CATCGATG <u>G</u> GAGAACGC <u>G</u> GCGAGATG TTGGCT <u>A</u> TGCGATCGATGAAGAACGCAGC <u>C</u> AAATG TTGGC <u>CA</u> TGCGATCGATGAAGAACGCAGC <u>C</u> AAATG
		<b>P2a<sup>HTT</sup></b> <b>P2b<sup>HTT</sup></b>	DNA probes complementary to T2 in a head-to-tail configuration
	<b>P2a<sup>TTT</sup></b> <b>P2b<sup>TTT</sup></b>		DNA probes for tail-to- tail configuration
		<b>NC</b>	Non-complementary DNA

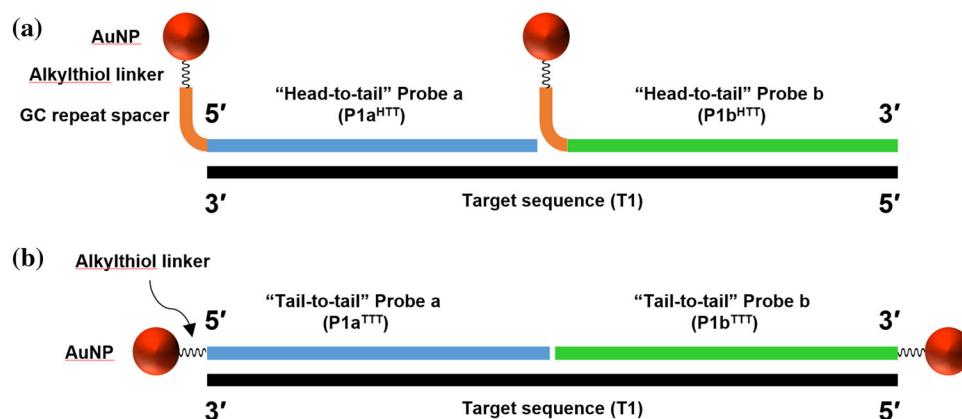
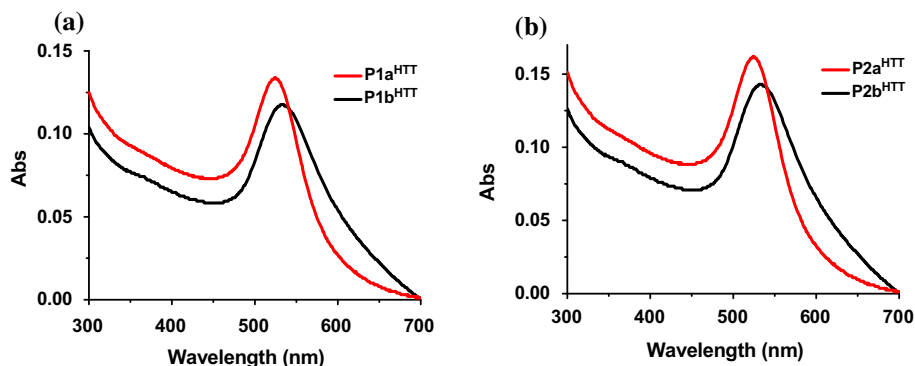


**Figure 1** Schematic diagrams illustrating the **a** head-to-tail (HTT) and **b** tail-to-tail (TTT) binding configurations of the DNA-AuNP conjugate probes to the complementary target single-stranded DNA. For brevity, only one example is shown for each

configuration: P1a<sup>HTT</sup> and P1b<sup>HTT</sup> in (a); or P1a<sup>TTT</sup> and P1b<sup>TTT</sup> in (b). Both pairs of probes are complementary to the T1 target sequence.

**Figure 2** UV–Vis absorption spectra of conjugates prepared using probes **a** P1a<sup>HTT</sup> and P1b<sup>HTT</sup>, **b** P2a<sup>HTT</sup>, and P2b<sup>HTT</sup>.



(P1a<sup>TTT</sup> and P1b<sup>TTT</sup>, P1c<sup>TTT</sup>, and P1d<sup>TTT</sup>) were prepared (Table 1). For sequence T2, one pair of each conjugate was prepared for each configuration (P2a<sup>HTT</sup> and P2b<sup>HTT</sup>, P2a<sup>TTT</sup>, and P2b<sup>TTT</sup>; Table 1).

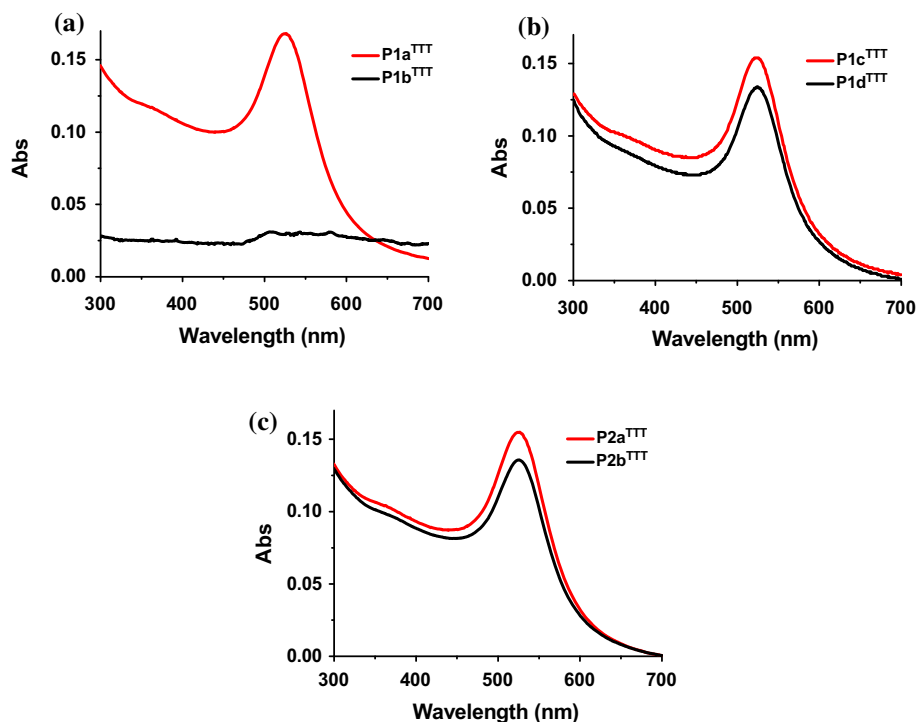
Following their preparation, the DNA-AuNP conjugate bearing the P1a<sup>HTT</sup> probe exhibited the expected deep red colour and a corresponding UV–Vis spectrum with a  $\lambda_{\max}$  at 525 nm (Fig. 2a), similar to  $\lambda_{\max}$  for unconjugated AuNP. However, for P1b<sup>HTT</sup>, a higher  $\lambda_{\max}$  (533 nm) and a broad tail towards the higher wavelengths was observed, which suggests the presence of aggregated AuNPs. DNA-AuNP colloids bearing the P2a<sup>HTT</sup> and P2b<sup>HTT</sup> probes also showed similar results (Fig. 2b), with P2b<sup>HTT</sup> showing a broad tail along with  $\lambda_{\max}$  at 533 nm. Both pairs of probes were thus unsuitable for further investigation.

Probes in the tail-to-tail configuration were then prepared, starting with the P1a<sup>TTT</sup> and P1b<sup>TTT</sup> pair. After DNA conjugation, the expected red colour and

a  $\lambda_{\max}$  of 525 nm were observed for colloid bearing the P1a<sup>TTT</sup> probe (Fig. 3a). However, despite several efforts to produce the conjugates of P1b<sup>TTT</sup> under various conditions, stable colloids could not be produced. The AuNPs precipitated during the NaCl addition step, resulting in only minimal amounts of suspended conjugates, as evidenced by the minimal UV–Vis absorbance. An alternative design was then attempted using the same sequence that was complementary to the T1 target sequence, but now differently divided into each probe (referenced as P1c<sup>TTT</sup> and P1d<sup>TTT</sup>; Table 1). This revised design led to the successful preparation of the DNA-AuNP conjugates with the expected optical properties (Fig. 3b). Based on these results, probes P2a<sup>TTT</sup> and P2b<sup>TTT</sup> were designed for T2 (Table 1), and the prepared conjugates were found to display the expected optical properties (Fig. 3c).

It was found that the prepared DNA-AuNP conjugates (P1c<sup>TTT</sup>, P1d<sup>TTT</sup>, P2a<sup>TTT</sup>, and P2b<sup>TTT</sup>) were

**Figure 3** UV–Vis absorption spectra of conjugates prepared using probes **a** P1a<sup>TTT</sup> and P1b<sup>TTT</sup>, **b** P1c<sup>TTT</sup> and P1d<sup>TTT</sup> and **c** P2a<sup>TTT</sup> and P2b<sup>TTT</sup>.



stable between a pH of 4 and 7, as evidenced by a lack of change in the UV–Vis spectra. Further, these conjugates were stable for up to two months if stored at 4 °C (at pH 7), though only for 3–4 days if stored at room temperature (in the UK, approximately 20 °C), as evidenced by UV–Vis spectroscopy.

These results suggest that to achieve stable conjugates, a minimum of 20 bases are required when DNA is conjugated to AuNP at 3' position of DNA, though the reason for this observation is unclear. The P1b<sup>TTT</sup> probe has been previously used successfully in other sensor platforms [19], but the current result nevertheless shows that the cross-compatibility of DNA probes between different applications cannot be assumed. Thus, the probe pair P1c<sup>TTT</sup>/P1d<sup>TTT</sup> complementary to T1, and P2a<sup>TTT</sup>/P2b<sup>TTT</sup> pair complementary to T2 were taken for further evaluation.

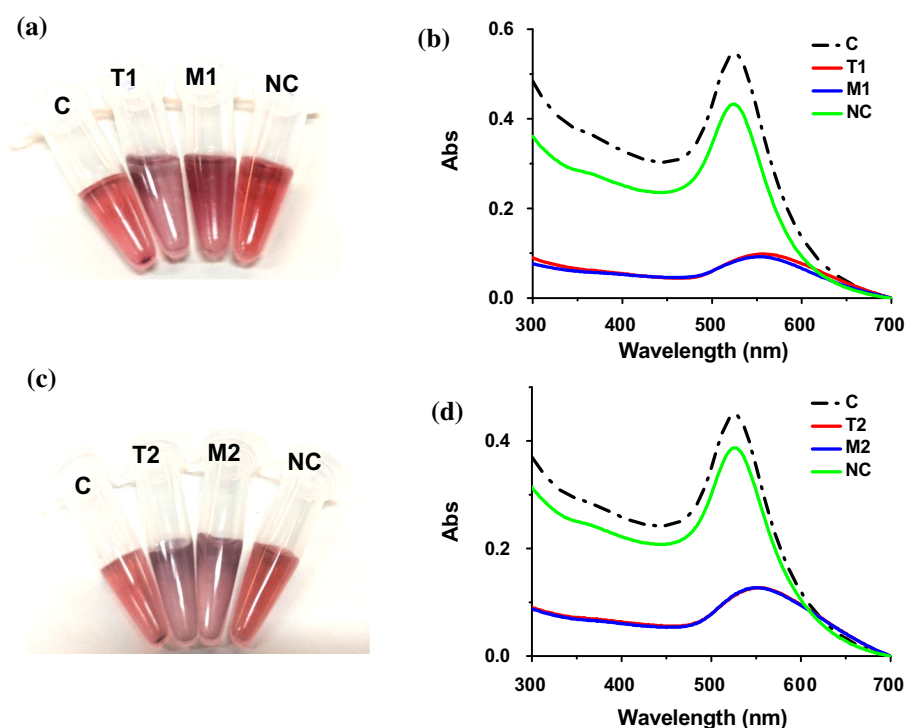
### Hybridisation against single-stranded DNA

In preliminary optimisation experiments, the hybridisation assays were carried out with ssDNA sequences as the analyte, which was added to a mixture consisting of each pair of complementary DNA–AuNP probes. Three types of analytes were tested (Table 1): (1) the 35-base target DNA strand fully complementary to their respective probes (i.e. either T1 or T2); (2) DNA sequences containing a

single base mismatch referred to as M1 and M2, but otherwise, identical to T1 or T2, respectively; (3) “non-complementary” DNA consisting of a randomly generated sequence of identical length and similar GC content to T1 and T2 (termed NC). In all cases, a mixture of equivalent concentrations of DNA–AuNP conjugates was prepared (to an OD of 0.7 @ 525 nm of each probe prior to mixing), to which the ssDNA analyte was added to give a final analyte concentration of 1 μM (corresponding to 200 pmol of analyte in 200 μL of the total assay mixture). In the negative control, only water was added as the analyte (henceforth referred to as “C” in all figures).

For the hybridisation experiments with the tail-to-tail configuration using probes P1c<sup>TTT</sup> and P1d<sup>TTT</sup> against T1, it was found that a hybridisation mixture with 1 M NaCl gave good hybridisation after 30 min. This result was evidenced by a visually observable colour change from a deep red to lilac and was corroborated by the UV–Vis spectrum that exhibited a  $\lambda_{\max}$  increase from 525 to 550 nm, a decrease in the absorbance at their respective  $\lambda_{\max}$  ( $A_{\max}$ ) from 0.6 to 0.1 (an approximately 80% reduction), and a broadening of the peak (Fig. 4a, b). In contrast, a negative control experiment where only water was added, no significant change in colour or the UV–Vis spectrum was observed. Similarly, the NC sequence gave no

**Figure 4** Photographs and UV–Vis spectra of the assay mixtures containing the DNA–AuNP conjugates and analyte for: **a, b** mixtures using P1c<sup>TTT</sup> and P1d<sup>TTT</sup> probes; and **c, d** mixtures using P2a<sup>TTT</sup> and P2b<sup>TTT</sup> probes. The key to the figure: C = negative control (buffer only, no DNA); T1, T2, M1, M2 and NC correspond to samples containing the analyte DNA listed in Table 1. The photographs show each assay carried out at a 200  $\mu$ L total volume.



significant change also, which confirms that probe binding is sequence specific. In the case of the mismatched sequence M1, a result similar to T1 was observed, which indicates this probe pair was able to bind and cannot differentiate this single mismatch from the fully complementary sequence (i.e. this is a false positive result).

A similar experiment was performed for P2a<sup>TTT</sup> and P2b<sup>TTT</sup> probes, against T2 or M2. Both these analyte sequences gave colour and spectroscopic changes corresponding to a positive result similar to the above (Fig. 4c, d). As before, negative controls consisting of the NC sequence or water only gave no change.

### Response time of hybridisation assay

The rapidity of the assay was then investigated. Here, using probes P2a<sup>TTT</sup> and P2b<sup>TTT</sup> against T2, it was found that a change in  $\lambda_{\max}$  from 525 to 548 nm, and decrease in the  $A_{\max}$  from 0.7 to 0.2, occurred after 15 min (Fig. 5c), with little further change even after 45 min (Fig. 5). This result thus shows that the 30-min incubation time previously used was, in fact, unnecessary, and thus, all subsequent assays were analysed after 15 min.

### Assay sensitivity against single-stranded DNA analyte

Based on the above results, DNA analyte T2 and DNA–AuNP conjugates prepared using probes P2a<sup>TTT</sup> and P2b<sup>TTT</sup> were taken for further study. A series of assays were carried out by adding between 0.1 and 10 pmol of T2 to the conjugates to test its sensitivity. These results were compared with a positive control with 200 pmol and negative control with water as the analyte. It was found that a visually observable colour change was produced with as little as 0.2 pmol of T2 (Fig. 6a), although the UV–Vis analysis showed that the  $\lambda_{\max}$  shift for this amount of analyte was smaller than for the higher amounts (10 nm vs. 25 nm, Fig. 6b). The UV–Vis spectrum corresponding to 0.1 pmol of T2 did show an  $\sim 50\%$  reduction in  $A_{\max}$  without an accompanying change of  $\lambda_{\max}$ , but this change could not be readily observed visually. Nevertheless, the overall visual transition is very sharp, spanning just one order of magnitude in the pmol–fmol range (i.e. 1.0 pmol was clearly positive, but 0.1 pmol was clearly negative), which equates to concentrations between 5 and 0.5 nM.



**Figure 5** **a** UV–Vis spectra of the assay mixtures containing the DNA–AuNP conjugates and target DNA analyte for P2a<sup>TTT</sup> and P2b<sup>TTT</sup> probes and **b** a graph of the corresponding  $\lambda_{\max}$  versus time. The photographs show C and T2 DNA analyte (200 pmol) assays after 1 and 15 min (**c** and **d**, respectively).

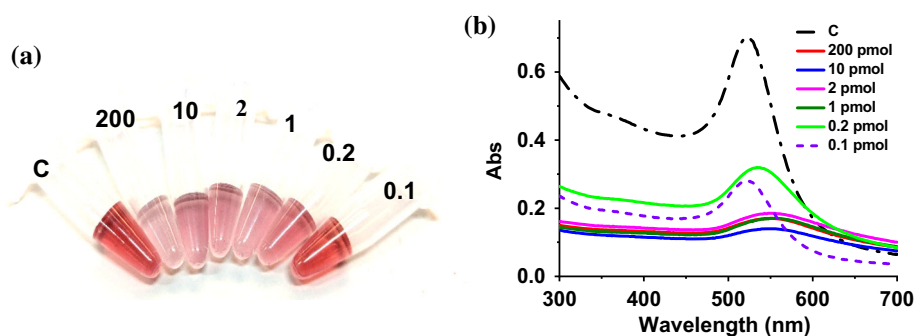
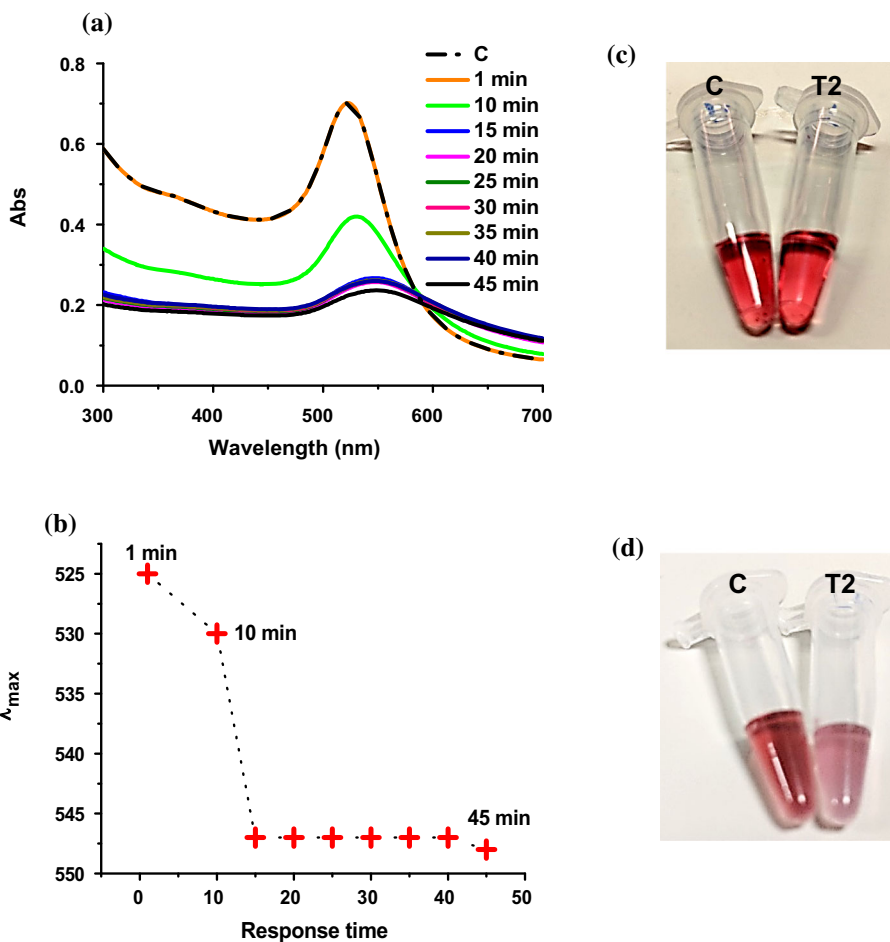


**Figure 6** **a** Photograph and **b** UV–Vis spectra of the assay mixtures containing the DNA–AuNP conjugates P2a<sup>TTT</sup> and P2b<sup>TTT</sup> and varying amounts of T2. The photograph shows each

assay carried out at a 200  $\mu\text{L}$  total volume, with the labels indicating the amount of T2 DNA added in pmol.

### Effect of mismatches on hybridisation efficiency

As the results with the single-base mismatch M2 sequence also gave a positive result, the tolerance of the assay (with probes P2a<sup>TTT</sup>/P2b<sup>TTT</sup>) against other mismatched sequences was investigated. For this

purpose, the assays were carried out with a series of analyte sequences bearing mismatches at multiple locations, referenced M2a to M2f (Table 1).

It was found that analyte sequence M2a, bearing three mismatches in series at the junction where the two probe sequences meet, also gave a false positive. This result was evidenced by a visually observable

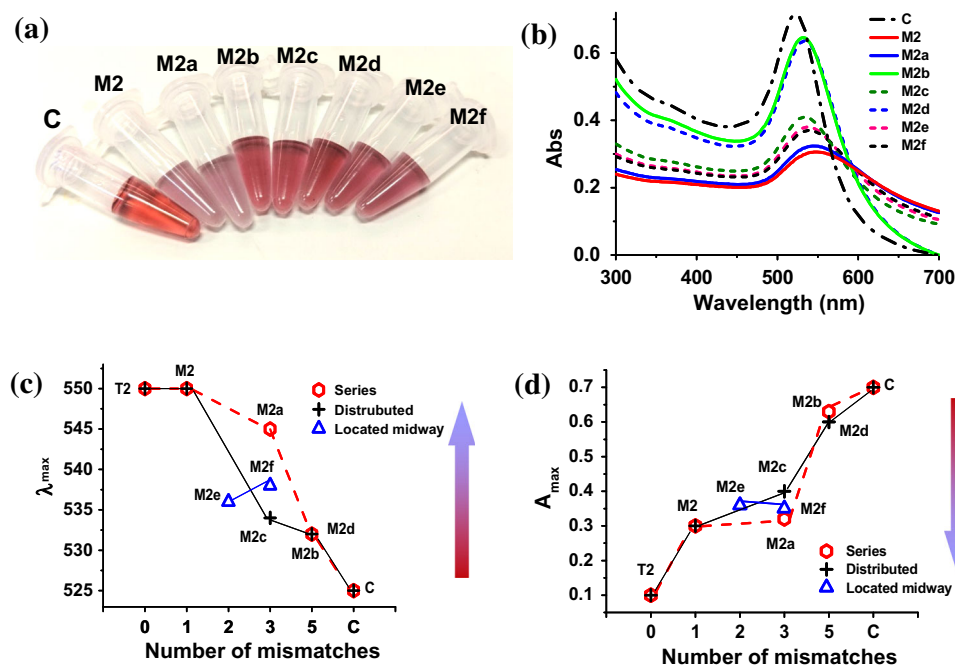


**Figure 7** **a** Photograph and **b** UV–Vis spectra of the assay mixtures containing the DNA–AuNP conjugates P2a<sup>TTT</sup> and P2b<sup>TTT</sup> and analyte sequences M2a to M2f, as well as M2 for comparison. Graphs of UV–Vis  $\lambda_{\max}$  (**c**) or  $A_{\max}$  (**d**) against the number of base-pair mismatches in the analyte sequences (the inset arrows show the visually observed colour change, and “C”

colour change, a UV–Vis  $\lambda_{\max}$  shift from 525 to 545 nm and a drop in  $A_{\max}$  similar to M2 (Fig. 7). The sequence with five mismatches in series (M2b) gave almost no change in visual appearance, which was confirmed spectroscopically by a small  $\lambda_{\max}$  increase to 531 nm and  $A_{\max}$  reduction of only 15%. Since this change was not visually distinguishable from the negative controls (C in Fig. 7 and NC in Fig. 4d), it was judged to be a “negative” result.

In contrast to M2a, if three mismatches were individually distributed throughout the analyte sequence (M2c), this gave a negative visual appearance that was similar to M2b (Fig. 7a). This observation was consistent with the UV–Vis spectrum showing a small  $\lambda_{\max}$  shift to 533 nm, although there was a significant decrease in the  $A_{\max}$  by 40% (Fig. 7b, d). The sequence M2d with five distributed mismatches was also negative, with a visual and spectral result that was similar to M2b.

The inability of these DNA–AuNP conjugates to differentiate either one or three mismatches in series at the meeting point of the two probes (M2 and M2a) can be rationalised by the binding stability of the

remaining complementary base pairs. It is known that DNA duplexes with more than  $\sim 12$  complementary base pairs typically exhibit melting temperatures ( $T_m$ ) well above 37 °C [36]. Since even three mismatches would allow both probes to bind with  $\geq 14$  serial base pairings, it would be expected that stable DNA hybridisation can still be achieved, which translates to a positive result. In comparison, M2c with three distributed mismatches gave a negative result. However, it is notable that five mismatches in series (M2b) gave a negative result, even though it would still theoretically give  $> 12$  base pairings in series. This result suggests that  $\geq 14$  serial base pairings are required in these conjugates, which could be due to the presence of AuNP hindering efficient hybridisation.

In the case of mismatches located midway within the sequence of each probe (M2e and M2f), these gave an ambiguous result that was mid-way between the positive and negative controls. An intermediate colour and intensity change were visually observed, consistent with the UV–Vis spectra that gave a  $\lambda_{\max}$  shift to 538 and 536 nm (for M2e and M2f, indicates the control reaction where water is added as the analyte). The photograph shows each assay carried out at a 200  $\mu$ L total volume, and the amount of mismatched DNA was kept at 200 pmol for consistency with the results observed for M2 (in “Hybridisation against single-stranded DNA” section).

respectively) and an  $A_{\max}$  decrease of  $\sim 48\%$  for both (Fig. 7d). Thus, though these mismatches could not be differentiated by eye, they could still be identified spectroscopically.

Assays based purely on direct hybridisation are known to have a limited ability to discriminate single base-pair mismatches due to the small difference in stability compared to a perfectly matched DNA duplex. Various modifications to the basic strategy such as employing specific interactions between Lambda exonuclease and a chemically modified DNA [37], double-stranded toehold exchange [38], and co-amplification at lower denaturation temperature [39] have been proposed to enhance the sensitivity of the assays towards one or more mismatches. However, these approaches increase the complexity of the assay and make it less suitable for field deployment.

### Assays against double-stranded DNA analytes

As a step towards biologically relevant diagnostics, the assay was next tested against dsDNA fragments. Here, the experiments consisted of dsDNA with the T2 sequence (referred henceforth as T2') and nanoparticle conjugates bearing probes P2a<sup>TTT</sup> and P2b<sup>TTT</sup>. The assay procedure was also modified such that the analyte was heated to 95 °C to induce the denaturation of the dsDNA [40] and enable subsequent probe hybridisation upon cooling. It was, however, observed that in contrast to ssDNA (see in "Response time of hybridisation assay" section), a more extended waiting period was needed for the assay to develop (30 vs. 15 min with ssDNA).

A range of analyte amounts was then tested from 0.2 to 200 pmol (in a 200  $\mu$ L final assay volume). In order to optimise the sensitivity, the concentration of NaCl in the assay mixtures were also varied (either 1.0 or 1.2 M) [41]. It was found that a visually observable positive result could be achieved at 10, and 1 pmol (corresponding to concentrations of 50 nM, and 5 nM, respectively) of T2', at each of the respective NaCl concentrations (Fig. 8a, c). These observations were supported by UV–Vis spectra showing both the expected increases in  $\lambda_{\max}$  and decreases in  $A_{\max}$ , typically by 20–25 nm and 40–50%, respectively, depending on the amount of analyte (Fig. 8b, d). However, even the best results obtained here were still fivefold less sensitive than the

equivalent experiment with ssDNA. This result is likely due to the competitive rebinding of the analyte ssDNA to its complementary strand upon cooling.

### Selectivity in the presence of non-complementary DNA

In order to demonstrate the selectivity of the assay in the presence of a large amount of non-complementary genomic DNA that would be present in any potential biologically derived sample, the optimised dsDNA assay was then carried out in the presence of calf thymus DNA (CT), as a model mixture of non-complementary dsDNA with a variety of lengths. Here, varying amounts of T2' dsDNA from 0.2 to 200 pmol were mixed with 2.6 mg of CT and tested.

Similar to the isolated dsDNA, quantities of T2' as low as 10 and 2 pmol (which equates to a concentration of 50 nM and 10 nM) gave a visually observable result, even in the presence of a considerable amount of CT, at 1 and 1.2 M (Fig. 9a) NaCl concentration, respectively. The UV–Vis spectra also showed the corresponding  $\lambda_{\max}$  increase from 525 to 540 nm, though the  $A_{\max}$  reduction, in this case, was more modest at 24% (Fig. 9b).

### Conclusion

In conclusion, we have demonstrated the detection of DNA fragments associated with *G. boninense* based on the application of sequence-selective aggregation of DNA–AuNP conjugates. A detailed optimisation was performed involving a range of analyte sequences and two assay configurations to detect ssDNA and dsDNA. The target DNA can be easily be visually identified down to a concentration of 0.2 pmol ssDNA or 2 pmol dsDNA. The sensitivity limit was maintained for the dsDNA even in the presence of a large excess of non-complementary DNA. This protocol is simple to implement and is relatively rapid (within 30 min), without the need for sophisticated equipment and specialist training. Indeed, only the mixing of several solutions at room temperature and heating to a single temperature is required.

These results represent the first steps towards the development of a nanoparticle-based assay for practical application in tropical agriculture. To this end, there is significant scope further improvement of the assay performance. The reported results were carried

**Figure 8** Photographs and UV–Vis spectra of the assay mixtures containing the DNA–AuNP conjugates P2a<sup>TTT</sup> and P2b<sup>TTT</sup> and varying amounts of T2', with 1.0 M (a, b) or 1.2 M (c, d) NaCl. The photographs show each assay carried out at a 200  $\mu$ L total volume, with the labels indicating the amount of T2' DNA added in pmol.

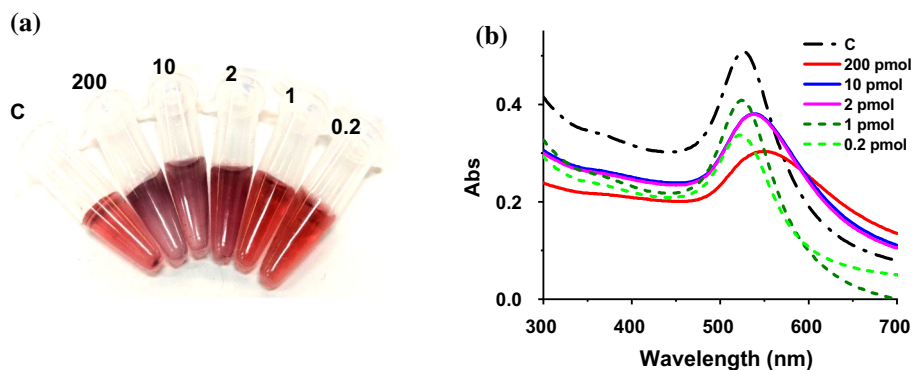
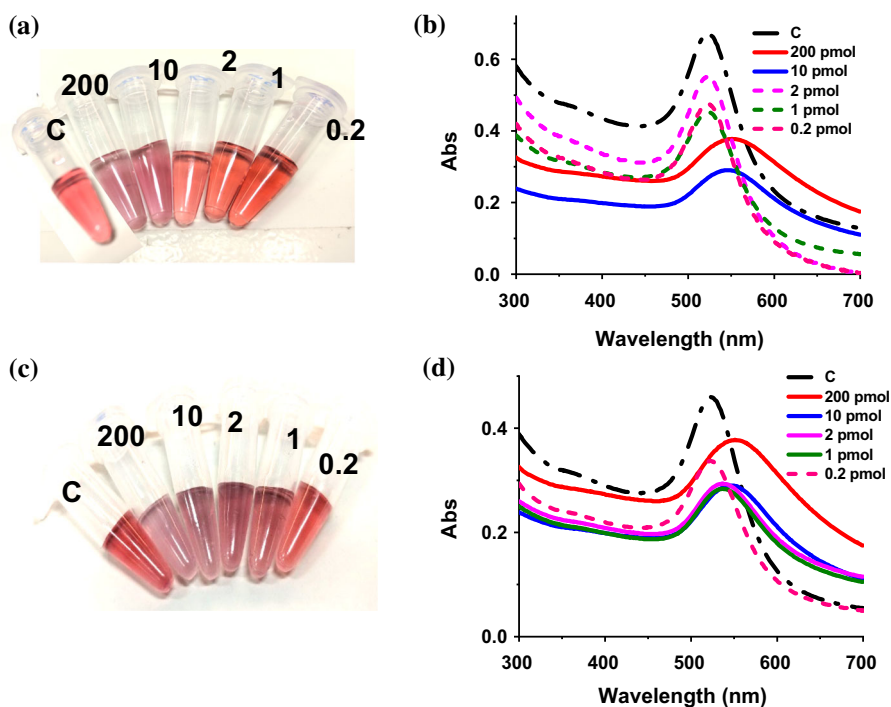


**Figure 9** a Photograph and b UV–Vis spectra of the assay mixtures containing the DNA–AuNP conjugates P2a<sup>TTT</sup> and P2b<sup>TTT</sup> and varying concentrations of T2' and in the presence of

CT with 1.2 M NaCl. The photograph shows each assay carried out at a 200  $\mu$ L total volume, with the labels indicating the amount of T2' DNA added in pmol.

out at a 200  $\mu$ L scale for the purposes of UV–Vis measurements. However, in a field application, scaling down the assay volumes by order of magnitude can be envisioned, and would still be sufficient for a visually observable result, while reducing the amount of analyte needed to the fmol range. It is noted that the current assay design is not able to differentiate a single mismatch or three mismatches in series. However, this limitation can be overcome by careful selection of sections of the ITS1 gene where there are large differences in sequence. The implementation of strand displacement strategies will also be able to achieve clearer differentiation between

sequences bearing mismatches [42–45]. The overall sensitivity of the assay could also be improved, especially with respect to dsDNA, through further modification of the basic approach, such as incorporating the capture of the nanoparticle aggregates on surfaces, by increasing the probe/target ratio or by increasing the size of the AuNP used [21, 32].

## Acknowledgements

The authors thank the British Council Newton Fund for support under Contract 216196834, the UK

Engineering and Physical Sciences Research Council for equipment support under Grants EP/K024485/1, and the HEFCE N8 Agri-food Network for travel funds.

## Compliance with ethical standards

**Conflict of interest** There are no conflict to declare.

**Open Access** This article is licensed under a Creative Commons Attribution 4.0 International License, which permits use, sharing, adaptation, distribution and reproduction in any medium or format, as long as you give appropriate credit to the original author(s) and the source, provide a link to the Creative Commons licence, and indicate if changes were made. The images or other third party material in this article are included in the article's Creative Commons licence, unless indicated otherwise in a credit line to the material. If material is not included in the article's Creative Commons licence and your intended use is not permitted by statutory regulation or exceeds the permitted use, you will need to obtain permission directly from the copyright holder. To view a copy of this licence, visit <http://creativecommons.org/licenses/by/4.0/>.

## References

- [1] Nambiappan B, Ismail A, Hashim N et al (2018) Malaysia: 100 years of resilient palm oil economic performance. *J Oil Palm Res* 30:13–25. <https://doi.org/10.21894/jopr.2018.0014>
- [2] Ho YW, Nawaw A (1985) *Ganoderma boninense* Pat. from basal stem rot of oil palm (*Elaeis guineensis*) in Peninsular Malaysia. *Pertanika* 8:425–428
- [3] Paterson RRM (2007) *Ganoderma* disease of oil palm—A white rot perspective necessary for integrated control. *Crop Prot* 26:1369–1376. <https://doi.org/10.1016/j.cropro.2006.11.009>
- [4] Utomo C, Niepold F (2000) Development of diagnostic methods for detecting *ganoderma*-infected oil palms. *J Phytopathol* 148:507–514. <https://doi.org/10.1046/j.1439-0434.2000.00478.x>
- [5] Hushiarian R, Yusof NA, Dutse SW (2013) Detection and control of *Ganoderma boninense*: strategies and perspectives. *Springerplus* 2:1–12. <https://doi.org/10.1186/2193-1801-2-555>
- [6] Guglielmo F, Bergemann SE, Gonthier P et al (2007) A multiplex PCR-based method for the detection and early identification of wood rotting fungi in standing trees. *J Appl Microbiol* 103:1490–1507. <https://doi.org/10.1111/j.1365-2672.2007.03378.x>
- [7] Ommelna BG, Jennifer AN, Chong KP (2012) The potential of chitosan in suppressing *Ganoderma boninense* infection in oil-palm seedlings. *J Sustain Sci Manag* 7:186–192
- [8] Markom MA, Shakaff AYM, Adom AH et al (2009) Intelligent electronic nose system for basal stem rot disease detection. *Comput Electron Agric* 66:140–146. <https://doi.org/10.1016/j.compag.2009.01.006>
- [9] Najmie M, Khalid K, Sidek A, Jusoh M (2011) Density and ultrasonic characterization of oil palm trunk infected by *Ganoderma boninense* disease. *Meas Sci Rev* 11:160–164. <https://doi.org/10.2478/v10048-011-0026-x>
- [10] Lelong CCD, Roger JM, Brégand S et al (2010) Evaluation of oil-palm fungal disease infestation with canopy hyperspectral reflectance data. *Sensors* 10:734–747. <https://doi.org/10.3390/s100100734>
- [11] Santoso H, Gunawan T, Jatmiko RH et al (2011) Mapping and identifying basal stem rot disease in oil palms in North Sumatra with QuickBird imagery. *Precis Agric* 12:233–248. <https://doi.org/10.1007/s11119-010-9172-7>
- [12] Djavanroodi F, Ahmadian H, Naseri R et al (2016) Experimental investigation of ultrasonic assisted equal channel angular pressing process. *Arch Civ Mech Eng* 16:249–255. <https://doi.org/10.1016/j.acme.2015.10.001>
- [13] Hashim IC, Shariff ARM, Bejo SK et al (2018) Classification for non infected and infected *Ganoderma boninense* of oil palm trees using ALOS PALSAR-2 backscattering coefficient. *IOP Conf Ser Earth Environ Sci* 169:012066. <https://doi.org/10.1088/1755-1315/169/1/012066>
- [14] Darmono TW, Suharyanto A (1995) Recognition of field materials of *Ganoderma* sp. associated with basal stem rot in oil palm by a polyclonal antibody. *Menara Perkeb* 63:15–22
- [15] Shamala S, Chris D, Sioban O, Idris AS (2006) Preliminary studies on the development of monoclonal antibodies against mycelia of *Ganoderma boninense*, the causal pathogen of basal stem rot of oil palm. *Malays J Microbiol* 2:30–34. <https://doi.org/10.21161/mjm.210605>
- [16] Madihah AZ, Idris AS, Rafidah AR (2014) Polyclonal antibodies of *Ganoderma boninense* isolated from Malaysian oil palm for detection of basal stem rot disease. *Afr J Biotechnol* 13:3455–3463. <https://doi.org/10.5897/AJB2013.13604>
- [17] Akanbi FS, Yusof NA, Abdullah J et al (2017) Detection of quinoline in *G. boninense*-infected plants using functionalized multi-walled carbon nanotubes: a field study. *Sensors* 17:1538. <https://doi.org/10.3390/s17071538>
- [18] Dutse SW, Yusof NA, Ahmad H et al (2014) An electrochemical biosensor for the determination of *Ganoderma boninense* pathogen based on a novel modified gold

- nanocomposite film electrode. *Anal Lett* 47:819–832. <https://doi.org/10.1080/00032719.2013.858261>
- [19] Hushiarian R, Yusof NA, Abdullah AH et al (2015) Facilitating the indirect detection of genomic DNA in an electrochemical DNA biosensor using magnetic nanoparticles and DNA ligase. *Anal Chem Res* 6:17–25. <https://doi.org/10.1016/j.ancr.2015.10.004>
- [20] Elghanian R, Storhoff JJ, Mucic RC et al (1997) Selective colorimetric detection of polynucleotides based on the distance-dependent optical properties of gold nanoparticles. *Science* (80-) 277:1078–1081. <https://doi.org/10.1126/science.277.5329.1078>
- [21] Storhoff JJ, Lucas AD, Garimella V et al (2004) Homogeneous detection of unamplified genomic DNA sequences based on colorimetric scatter of gold nanoparticle probes. *Nat Biotechnol* 22:883–887. <https://doi.org/10.1038/nbt977>
- [22] Li F, Zhang H, Dever B et al (2013) Thermal stability of DNA functionalized gold nanoparticles. *Bioconjug Chem* 24:1790–1797. <https://doi.org/10.1021/bc300687z>
- [23] Valentini P, Pompa PP (2013) Gold nanoparticles for naked-eye DNA detection: smart designs for sensitive assays. *RSC Adv* 3:19181–19190. <https://doi.org/10.1039/c3ra43729a>
- [24] Li G, Zhu L, Wu Z et al (2016) Digital concentration readout of DNA by absolute quantification of optically countable gold nanorods. *Anal Chem* 88:10994–11000. <https://doi.org/10.1021/acs.analchem.6b02712>
- [25] Wu Z, Yang R, Zu D, Sun S (2017) Microscopic differentiation of plasmonic nanoparticles for the ratiometric readout of target DNA. *Sci Rep* 7:1–9. <https://doi.org/10.1038/s41598-017-15256-1>
- [26] Jyoti A, Pandey P, Pal Singh S et al (2010) Colorimetric detection of nucleic acid signature of shiga toxin producing *Escherichia coli* using gold nanoparticles. *J Nanosci Nanotechnol* 10:4154–4158. <https://doi.org/10.1166/jnn.2010.2649>
- [27] Tan YN, Lee KH, Su X (2011) Study of single-stranded DNA binding protein–nucleic acids interactions using unmodified gold nanoparticles and its application for detection of single nucleotide polymorphisms. *Anal Chem* 83:4251–4257. <https://doi.org/10.1021/ac200525a>
- [28] Tan YN, Lee KH, Su X (2013) A study of DNA design dependency of segmented DNA-induced gold nanoparticle aggregation towards versatile bioassay development. *RSC Adv* 3:21604–21612. <https://doi.org/10.1039/c3ra44661a>
- [29] Liang K, Zhai S, Zhang Z et al (2014) Ultrasensitive colorimetric carcinoembryonic antigen biosensor based on hyperbranched rolling circle amplification. *Analyst* 139:4330–4334. <https://doi.org/10.1039/c4an00417e>
- [30] Chen C, Luo M, Ye T et al (2015) Sensitive colorimetric detection of protein by gold nanoparticles and rolling circle amplification. *Analyst* 140:4515–4520. <https://doi.org/10.1039/c5an00485c>
- [31] Li F, Wang J, Lai Y et al (2013) Ultrasensitive and selective detection of copper (II) and mercury (II) ions by dye-coded silver nanoparticle-based SERS probes. *Biosens Bioelectron* 39:82–87. <https://doi.org/10.1016/j.bios.2012.06.050>
- [32] Rani E, Mohshim SA, Ahmad MZ et al (2019) Polymer pen lithography-fabricated DNA arrays for highly sensitive and selective detection of unamplified *Ganoderma boninense* DNA. *Polymers (Basel)* 11:561. <https://doi.org/10.3390/polym11030561>
- [33] Sakamoto A, Mikawa T, Murase M, Tanaka A, Kuran R (2001) Method for detecting a disease germ of oil palm, *Ganoderma boninense* and detection primer. Patent JP 2001314199-A1
- [34] Badotti F, De Oliveira FS, Garcia CF et al (2017) Effectiveness of ITS and sub-regions as DNA barcode markers for the identification of Basidiomycota (Fungi). *BMC Microbiol* 17:1–12. <https://doi.org/10.1186/s12866-017-0958-x>
- [35] Sun W, Jiang T, Lu Y et al (2014) Cocoon-like self-degradable DNA nanoclew for anticancer drug delivery. *J Am Chem Soc* 136:14722–14725. <https://doi.org/10.1021/ja5088024>
- [36] de Bruin D, Bossert N, Aartsma-Rus A, Bouwmeester D (2018) Measuring DNA hybridization using fluorescent DNA-stabilized silver clusters to investigate mismatch effects on therapeutic oligonucleotides. *J Nanobiotechnol* 16:1–8. <https://doi.org/10.1186/s12951-018-0361-2>
- [37] Wu T, Xiao X, Zhang Z, Zhao M (2015) Enzyme-mediated single-nucleotide variation detection at room temperature with high discrimination factor. *Chem Sci* 6:1206–1211. <https://doi.org/10.1039/c4sc03375b>
- [38] Chen SX, Zhang DY, Seelig G (2013) Conditionally fluorescent molecular probes for detecting single base changes in double-stranded DNA. *Nat Chem* 5:782–789. <https://doi.org/10.1038/nchem.1713>
- [39] Li J, Wang L, Mamon H et al (2008) Replacing PCR with COLD-PCR enriches variant DNA sequences and redefines the sensitivity of genetic testing. *Nat Med* 14:579–584. <https://doi.org/10.1038/nm1708>
- [40] Wang X, Lim HJ, Son A (2014) Characterization of denaturation and renaturation of DNA for DNA hybridization. *Environ Health Toxicol* 29:e2014007. <https://doi.org/10.5620/eht.2014.29.e2014007>
- [41] Sato K, Hosokawa K, Maeda M (2003) Rapid aggregation of gold nanoparticles induced by non-cross-linking DNA hybridization. *J Am Chem Soc* 125:8102–8103. <https://doi.org/10.1021/ja034876s>
- [42] Xu G, Lai M, Wilson R et al (2019) Branched hybridization chain reaction—using highly dimensional DNA

- nanostructures for label-free, reagent-less, multiplexed molecular diagnostics. *Microsyst Nanoeng* 5:37. <https://doi.org/10.1038/s41378-019-0076-z>
- [43] Wang JY, Liu Y, Hofmann S, Kovac J (2012) Influence of nonstationary atomic mixing on depth resolution in sputter depth profiling. *Surf Interface Anal* 44:569–572. <https://doi.org/10.1002/sia.3855>
- [44] Yao D, Song T, Sun X et al (2015) Integrating DNA-strand-displacement circuitry with self-assembly of spherical nucleic acids. *J Am Chem Soc* 137:14107–14113. <https://doi.org/10.1021/jacs.5b07453>
- [45] Song T, Xiao S, Yao D et al (2014) An efficient DNA-fueled molecular machine for the discrimination of single-base changes. *Adv Mater* 26:6181–6185. <https://doi.org/10.1002/adma.201402314>

**Publisher's Note** Springer Nature remains neutral with regard to jurisdictional claims in published maps and institutional affiliations.